Check for updates

# An alternative electrochemical approach for toluene detection with ZnO/MgO/Cr$_2$O$_3$ nanofibers on a glassy carbon electrode for environmental monitoring†

M. M. Alam, [iD] *[a] Abdullah M. Asiri,[bc] M. T. Uddin, [iD] [a] Mohammed M. Rahman*[bc] and M. A. Islam[a]

*In situ* fabrication of a sensitive electrochemical sensor using a wet-chemically prepared ternary ZnO/MgO/Cr$_2$O$_3$ nanofiber (NF)-decorated glassy carbon electrode (GCE) with Nafion adhesive was the approach of this study. The resultant NFs were characterized by various tools, such as powder X-ray diffraction (XRD), X-ray photoelectron spectroscopy (XPS), field emission scanning electron microscopy (FESEM), energy-dispersive X-ray spectroscopy (EDS), Fourier transform infrared spectroscopy (FTIR), Brunauer–Emmett–Teller (BET) surface area analysis, and ultraviolet–visible spectroscopy (UV/Vis). The analytical parameters of the proposed toluene sensor were characterized as follows: good sensitivity (23.89 µA µM$^{-1}$ cm$^{-2}$), a lower limit of detection (LOD; 95.59 ± 1.5 pM), a limit of quantification (LOQ; 318.63 ± 2.0 pM), efficient response time (18 s), and the dynamic range (LDR) for toluene detection of 0.1 nM–0.01 mM. The real-time application of the sensor is to protect the environmental ecosystem, as well as the public health from the harmful effects of toluene. In an environmental application, the toluene sensor exhibited good reproducibility, robustness, LOD, LOQ, and good reliability, which are discussed in detail and compared to the literature.

## Introduction

In general, the organic volatile compounds emitted from industrial effluents, automobile exhaust, incineration, and other processes are responsible for the long- and short-term adverse health effects. The health and environmental organizations have designed the maximum contamination limit of these volatile organic compounds in the indoor and outdoor environments.[1] Among these volatile organic compounds, toluene (C$_7$H$_8$) is widely used in the chemical industry and is found to be neurotoxin, which is harmful to the human body at low concentrations.[2] Toluene is used in many applications, such as flame retardants, fuel systems, antifreeze, rust preservatives, metal cleaners, adhesives, glues, nail polish, thinners, varnishes, and paints.[3] Besides this, toluene is applied as a raw material to produce detergents, perfumes, dyes, inks, plastics, medicines and various chemicals.[4,5] Due to the toxicity of toluene, the impact on public health and environmental ecosystem is hazardous. The small amount of (less than 200 ppm) toluene inhalation is responsible for numerous illnesses in humans, such as dilated pupils, exhaustion, anxiety, euphoria, weakness, irritation in the eyes and nose, tingling in the skin and dermatitis, lacrimation, confusion, insomnia, and fatigue.[6,7] As toluene is a flammable and toxic, reliable detection methods are desired to protect the public health and environment.

Of late, the electrochemical sensors using sensing elements (such as semi-conductive metal oxides) are becoming popular in the detection of environmental toxic chemicals.[8–10] Numerous metal oxides, including Cr$_2$O$_3$,[11] ZnO,[12] SnO$_2$,[13] WO$_3$,[14] α-Fe$_2$O$_3$,[15] Co$_3$O$_4$,[16] In$_2$O$_3$,[17] and the hybrid composite of these metal oxides[18,19] have been investigated as sensing substrates of toluene. However, most research studies have been executed to detect toluene in the gaseous phase. As toluene has a wide range of applications, there is a great risk of contamination of the aqueous environment. Therefore, this study was approached to develop a toluene sensor with semi-conductive metal oxide nanomaterials, which are capable of the detection of the toluene target in an aqueous medium. The selectivity of the traditional sensor is a great challenge, because similar elements exhibit multi-selectivity. To overcome this drawback, two or

*a Department of Chemical Engineering and Polymer Science, Shahjalal University of Science and Technology, Sylhet 3100, Bangladesh. E-mail: alam-mahmud@hotmail.com*

*b Department of Chemistry, King Abdulaziz University, Faculty of Science, P.O. Box 80203, Jeddah 21589, Saudi Arabia. E-mail: mmrahman@kau.edu.sa*

*c Center of Excellence for Advanced Materials Research (CEAMR), King Abdulaziz University, P.O. Box 80203, Jeddah 21589, Saudi Arabia*

† Electronic supplementary information (ESI) available. See DOI: 10.1039/d0ra08577d

multi-metal oxides are utilized as the sensing mediator in this modern research approach. Also, a change in the interfacial resistance due to the formation of a heterojunction resulted in the improved performance of the sensors.[20] It has been reported previously that the binary $ZnO-SnO_2$ NFs,[21] $ZnO-Cr_2O_3$ NRs,[22] and $ZnO-In_2O_3$ NFs[23] reliably detect ethanol, trimethylamine, and trimethylamine, respectively. Recently, a few research studies based on the composite metal oxides have been reported to reliably detect toluene in an aqueous medium. So far, there still needs to be further improvements to develop composite metal oxide-based sensors. Among various metal oxides, ZnO is a semi-conductor with advantageous properties, such as 3.37 eV optical band gap, 60 meV free-exciton binding energy, 300 $cm^{-1}$ optical gain, mechanical and thermal stability.[24] Therefore, considering its ferroelectric, piezoelectric, optical, electrical and magnetic properties, ZnO is a strong candidate to use in the advanced electrochemical device application.[25] It has been reported that MgO is another potential nanomaterial (metal oxides), and is capable of improving the efficiency of the solar cell.[26] Besides this, $Cr_2O_3$ is an efficient metal oxide used as a gas-sensing element.[27]

In this study, $ZnO/MgO/Cr_2O_3$ NFs have been considered for its favorable structural, optical and physicochemical properties in terms of its permeability, high porosity, high-stability, and large-active surface area, which are dependent on the reactant precursors (chromium nitrate, zinc nitrate, and magnesium sulphate), and the morphology used in the synthesis of $ZnO/MgO/Cr_2O_3$ NFs at low temperature in the alkaline phase. The nanofibers of $ZnO/MgO/Cr_2O_3$ were prepared using the co-precipitation (wet-chemical) method, applying $NH_4OH$ as the precipitating agent. This wet-chemical preparation has effectual advantages, such as high-porosity, one-step reaction, ease of preparation, precious temperature controlling and facile handling facilities. The resulting properties of the $ZnO/MgO/Cr_2O_3$ NFs (chemical, electrical, optical, and structural morphology) have a great significance in terms of the scientific aspect compared to the un-doped nanomaterials. The conductivity of this ternary $ZnO/MgO/Cr_2O_3$ NFs enhances its non-stoichiometric oxygen vacancies. The energy associated with oxygen vacancies and metal interstitials in the doped-semiconductors is low, and it generated the elevated conductivity of the $ZnO/MgO/Cr_2O_3$ NFs compared to other un-doped semiconductors. Besides this, the $ZnO/MgO/Cr_2O_3$ NFs have attracted significant research interest owing to their probable applications in the fabrication of a biochemical detector, electron-field emission sources, hybrid-composites, and sensor devices. Moreover, due to the high reactive inter-surface area of the $ZnO/MgO/Cr_2O_3$ NFs on GCE, it possesses the high conductivity, as well as current density in the electrochemical analysis.[28–30]

Therefore, this approach involved the fabrication of a selective toluene sensor applying ternary $ZnO/MgO/Cr_2O_3$ NFs on GCE. The wet-chemically prepared $ZnO/MgO/Cr_2O_3$ NFs were decorated on GCE using Nafion adhesive as a thin film, resulting in the proposed toluene sensor. The fabricated toluene sensor exhibited good performances in terms of its analytical parameters, such as good sensitivity, extended dynamic range (LDR) for toluene detection, the significant lower limit for

detection (LOD), efficient response time, precious reproducibility and long-term performing ability in the electrochemical sensing performance of toluene in the buffer phase. To the best of our knowledge, this is the first time that the synthesized ternary $ZnO/MgO/Cr_2O_3$ NFs were applied onto GCE to detect unsafe toluene levels by an electrochemical approach. This approach to the development of an electrochemical sensor for the reliable detection of environmentally unsafe toxic chemicals should be a great advantage in the environmental sector.
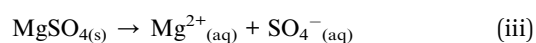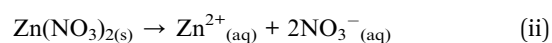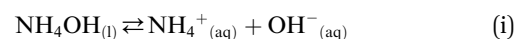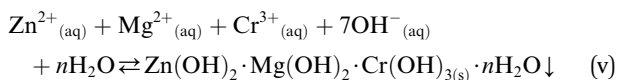
## Experimental section

### Chemicals and reagents

Analytical grade inorganic salts, such as $Cr(NO_3)_3 \cdot 9H_2O$, $MgSO_4 \cdot 7H_2O$, and $Zn(NO_3)_2 \cdot 6H_2O$, were purchased from the Sigma-Aldrich company (USA), and used directly to prepare $ZnO/MgO/Cr_2O_3$ NFs. To perform this study, the toxic chemicals, including 2-acetylpyridin, M-xylol, 3-methylaniline, zimtaldehyde, 1,4-dioxane, toluene, chlorobenzene, hydroquinone, and paracetamol, were also obtained from Sigma-Aldrich. Besides this, concentrated ammonia, the Nafion adhesive, mono- and disodium phosphate were supplied by Merck Germany to complete this study.

### Synthesis of $ZnO/MgO/Cr_2O_3$ nanofibers by wet-chemical method

The co-precipitation method was used to prepare the nano-structure materials of the doped/un-doped metal oxides with distinct surface-sensitive morphological structure. The $ZnO/MgO/Cr_2O_3$ NFs were prepared to apply this wet-chemical method in the high alkaline phase. This process consists of three sequential parts: (i) co-precipitation of the metal ions in the form of metal hydroxides; (ii) separation of the obtained metal hydroxides, followed by drying in an oven; and (iii) calcination of the metal hydroxides, which was performed in a muffle furnace under pure oxygen flow. Following these procedures, 0.1 M solutions of $MgSO_4 \cdot 7H_2O$, $Zn(NO_3)_2 \cdot 6H_2O$, and $Cr(NO_3)_3 \cdot 9H_2O$ were prepared in three separate 100.0 mL volumetric flasks using de-ionized water. After that, a 50.0 mL aliquot of the solution from each volumetric flask was taken into a 250.0 mL beaker, and heated at 80 °C on a hot-plate with continuous magnetic stirring. Subsequently, the pH of the mixture was maintained at 10.5 by adding 0.1 M $NH_4OH$ solution drop-wise. It has been considered that metal ions are co-precipitated quantitatively in the form of metal hydroxides at pH 10.5. After that, the obtained white precipitate of the metal hydroxides was filtrated and washed with water successively to remove the impurities and unreacted metal ions (if any). Finally, the obtained crystal mass was dried at 120 °C in an oven overnight. The probable reaction scheme is as follows:

$$NH_4OH_{(l)} \rightleftharpoons NH_4^+{}_{(aq)} + OH^-{}_{(aq)} \qquad (i)$$

$$Zn(NO_3)_{2(s)} \rightarrow Zn^{2+}{}_{(aq)} + 2NO_3^-{}_{(aq)} \qquad (ii)$$

$$MgSO_{4(s)} \rightarrow Mg^{2+}{}_{(aq)} + SO_4^-{}_{(aq)} \qquad (iii)$$

$$Cr_2(NO_3)_{3(s)} \rightarrow 2Cr^{3+}_{(aq)} + 3NO_3^-_{(aq)} \qquad (iv)$$

$$Zn^{2+}_{(aq)} + Mg^{2+}_{(aq)} + Cr^{3+}_{(aq)} + 7OH^-_{(aq)}$$
$$+ nH_2O \rightleftharpoons Zn(OH)_2 \cdot Mg(OH)_2 \cdot Cr(OH)_{3(s)} \cdot nH_2O \downarrow \qquad (v)$$
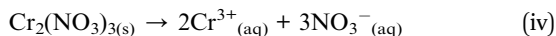
The precipitation of the metal hydroxide depends on the solubility-product-constant $K_{sp}$ [$K_{sp} = 3 \times 10^{-27}$ for $Zn(OH)_2$, $K_{sp} = 5.61 \times 10^{-12}$ for $Mg(OH)_2$, and $K_{sp} = 6.3 \times 10^{-31}$ for $Cr(OH)_3$].[31] With the dropwise addition of $NH_4OH$ into a beaker, the $OH^-$ concentration in the solution was increased gradually and the pH increased. As the $K_{sp}$ value of $Cr(OH)_3$ is lower compared to other existing metal hydroxides, the precipitation was initiated first and the small nuclei of crystallites were formed to generate the crystal formation. The resulting crystallites of $Cr(OH)_3$ were aggregated together to form a large crystallite. As the pH of the solution was continuously increased gradually, the 2nd lowest $K_{sp}$ value of $Zn(OH)_2$ also began to precipitate, and was followed by the adsorption on the crystallites of $Cr_2(OH)_3$. Subsequently, the 3rd $Mg(OH)_2$ with the highest $K_{sp}$ value was precipitated similarly. The resultant crystals of the nanomaterials were separated from the aqueous phase, and washed successively with deionized water. Then, the washed nanocrystals of the obtained metal hydroxides were dried in an oven overnight at 120 °C. After that, the dry nanocrystals were ground with a pestle and mortar, and followed by calcination at 500 °C for 6 hours in the muffle furnace. During the calcination process, the metal hydroxides were oxidized to metal oxides in the presence of flowing oxygen gas. The probable reaction involved in the muffle furnace is as follows:

$$Zn(OH)_2 \cdot Mg(OH)_2 \cdot Cr(OH)_{3(s)} + {}^3\!/_2 O_2 \rightarrow ZnO \cdot MgO \cdot Cr_2O_3 + {}^7\!/_2 H_2O \qquad (vi)$$
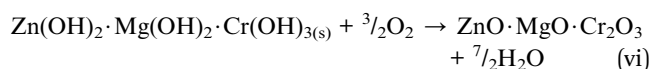
### Instrumentation

The investigation of the binding energy and ionization states of the existing atoms of the ZnO/MgO/Cr$_2$O$_3$ NFs were evaluated by XPS analysis performed on a K-α1 spectrometer (Thermo scientific, K-α1 1066) with an excitation radiation source (A1 Kα1, beam spot size = 300.0 μm, pass energy = 200.0 eV, pressure ∼ 10–8 torr). The photosensitivity and existing functional groups of the synthesized ZnO/MgO/Cr$_2$O$_3$ NFs were evaluated by the application of UV-Vis (Thermo Scientific) and FTIR (Thermo Scientific NICOLET iS50, Madison, WI, USA) spectroscopic analysis. The structural morphology and elemental compositions (shape, size, and structure) of the synthesized ZnO/MgO/Cr$_2$O$_3$ NFs were inspected by FESEM (JEOL, JSM-7600F, Japan) furnished with EDS. The phase crystallinity of the nanomaterial is an important measurable characteristic, and it is able to determine the unit cell dimension. Therefore, the phase crystallinity was studied by powder X-ray diffraction. The N$_2$ adsorption–desorption isotherms were carried out by the 3Flex analyzer (Micromeritics, USA) at 77.0 K. The specific surface area (SBET) was calculated using multi-point adsorption data from the linear segment of the N$_2$ adsorption isotherms using BET theory. Finally, the electrochemical detection was performed by a Keithley electrometer (USA).

### Fabrication of working electrode with NFs

The working electrode of the proposed sensor is the dominating part, and was fabricated by modification of a GCE with ZnO/MgO/Cr$_2$O$_3$ NFs with the help of the Nafion adhesive. For the fabrication of this electrode, a slurry of NFs in ethanol was deposited on the GCE with a surface area of 0.0316 cm$^2$ to form a layer of thin film. Then, it was kept at the ambient conditions of the laboratory to dry completely. To enhance the working duration of the electrode, a few drops of Nafion adhesive was put on the surface of the NFs layer on the GCE to boost its stability. After that, the modified GCE was kept in an oven at 35.0 °C for an adequate amount of time to dry it again. An electrochemical cell (chemical sensor) was assembled by connecting the ZnO/MgO/Cr$_2$O$_3$ NFs/GCE and Pt-wire through the Keithley electrometer to perform as the working and counter electrodes, respectively. The toluene solution at a concentration range of 0.1 nM to 0.1 mM was prepared in deionized water, and applied as the targeted analyte for electrochemical characterization of the sensor. A plot showing the current *versus* concentration of toluene was explored and denoted as a calibration curve, which was found to be linear and identified by regression coefficient $R^2$. The slope of the calibration-curve and surface area of GCE were used to calculate the sensor sensitivity. By marking a linear segment on the calibration-curve, the dynamic range of detection (LDR) was obtained. The lower limit (LOD) and quantification limit (LOQ) for toluene detection were calculated using a signal/noise (S/N) ratio of 3. During the electrochemical analysis, the buffer solution in the investigating beaker was kept as 10.0 mL as a constant. It should be mentioned that the Keithley electrometer (USA) is a simple two-electrode system device.

## Result and discussion

### XPS analysis of the ZnO/MgO/Cr$_2$O$_3$ NFs

The binding energy and ionization states of the existing atoms in the prepared ZnO/MgO/Cr$_2$O$_3$ NFs were investigated by applying XPS, as illustrated in Fig. 1. As seen in Fig. 1(a), the Zn 2p level orbital is split into two symmetric spin orbitals positioned at 1022.5 and 1045.5 eV, corresponding to Zn 2p$_{3/2}$ and Zn 2p$_{1/2}$, respectively. The spin energy separation between the Zn 2p$_{3/2}$ and Zn 2p$_{1/2}$ orbitals is 23.0 eV, which is recognized for the Zn$^{2+}$ ionization state in the ZnO/MgO/Cr$_2$O$_3$ NFs, as confirmed by previously reported articles.[31–33] The resultant XPS peak is fitted with the deconvolution data of Zn$^{2+}$, as shown in Fig. 1(a). Besides this, the O 1s XPS spectra (as in Fig. 1(b)) were fitted at 532.0 eV, which is associated with the lattice oxygen in the prepared NFs and expressed O$^{2-}$ ionization state.[34,35] Moreover, Fig. 1(c) presents the XPS spectra of the core level Cr 2p orbital, which further dissociates into the spin orbitals of Cr 2p$_{3/2}$ and Cr 2p$_{1/2}$, and are located at 578.0 and 588.0 eV, respectively. The spin energy separation of Cr 2p$_{3/2}$ and Cr 2p$_{1/2}$ is 10.0 eV, and can be ascribed to Cr$^{3+}$ in the ZnO/MgO/Cr$_2$O$_3$ NFs.[36] Furthermore, the high-resolution XPS spectra of Mg 2p (as in Fig. 1(d)) are located at 50.4 eV, which is a characteristic value for the Mg$^{2+}$ oxidation, as reported earlier.[37,38]

## The structural morphology of the ZnO/MgO/Cr$_2$O$_3$ NFs analyzed by FESEM

In this approach, the lower and higher magnification FESEM images of ZnO/MgO/Cr$_2$O$_3$ NFs are demonstrate in Fig. 2(a and b). As revealed from Fig. 2(a and b), the prepared nano-composite exhibited the fibre-like complex morphology. Therefore, it can be concluded that the prepared ternary mixed metal oxide has fiber-shaped morphology with the irregular arrangement. The similar morphology of the nanomaterials with ZnO are reported elsewhere.[39,40] The average cross-section diameter of the fiber is 68.7 nm, which was obtained in a range of 60.0 to 85 nm. The elemental analysis of ZnO/MgO/Cr$_2$O$_3$ executed by EDS, as in Fig. 2(c and d) and Fig. 2(c), confirmed the nanofiber morphology of the synthesized ZnO/MgO/Cr$_2$O$_3$ composites. The elemental analysis obtained from EDS provided evidence of the existence of only O, Zn, Mg, and Cr, and any peak due to impurities was not detected. The elemental composition of the ZnO/MgO/Cr$_2$O$_3$ NFs is 46.66%, 9.21%, 27.14%, and 16.99% corresponding to O, Mg, Cr and Zn, respectively.

## Optical characterization of ZnO/MgO/Cr$_2$O$_3$ NFs

The existing functional groups of the ZnO/MgO/Cr$_2$O$_3$ NFs were identified by FTIR spectra, which are shown in Fig. 3(a). The FTIR investigation was executed in the 450–4000 cm$^{-1}$ range, as shown in Fig. 3(a), and the absorption bands recorded at 460 and 620 cm$^{-1}$ correspond to the Zn–O and Mg–O optical stretching vibrations, respectively.[41,42] Besides this, the observed FTIR peaks at 1100, 1650 and 3300 cm$^{-1}$ were obtained for the stretching vibration of Mg–OH, and the bending and bonding vibration of the OH group, respectively.[43,44]

The photo-absorption of the ZnO/MgO/Cr$_2$O$_3$ NFs was investigated by applying UV-Vis spectroscopic analysis in the range of 300–800 nm, as shown in Fig. 3(b), which displayed a visible adsorption band at 364 nm due to the transition of valence electrons from the low to high energy levels.[45] Therefore, the optical band gap of the ZnO/MgO/Cr$_2$O$_3$ NFs was calculated following eqn (vii), and the obtained bandgap is 3.41 eV:

$$E_{bg} \text{ (eV)} = 1240/\lambda \tag{vii}$$

where $E_{bg}$ is the band-gap energy, and $\lambda$ is labeled as the highest absorbed wave-length.

The crystalline phases of the ZnO/MgO/Cr$_2$O$_3$ NFs were inspected using X-ray powder diffraction (XRD) analysis using a Cu-K$\alpha$ radiation source at 1.5406 Å in the range of $2\theta$ (20°–80°), as illustrated in Fig. 3(c), which consists of the ZnO, MgO, and Cr$_2$O$_3$ crystalline phases only. As shown in Fig. 3(c), the diffracted peaks of ZnO are (100), (002), (101), (102), (110), (103), (112) and (102) planes, which were identified by JCPDS no. 065-3411 and previous articles on ZnO.[46,47] Besides this, the crystalline phases of MgO are (220), (222), (400) and (422). These reflected peaks of MgO were identified by JCPDS no. 004-0829 and previous authors.[48,49] Moreover, several reflected XRD peaks
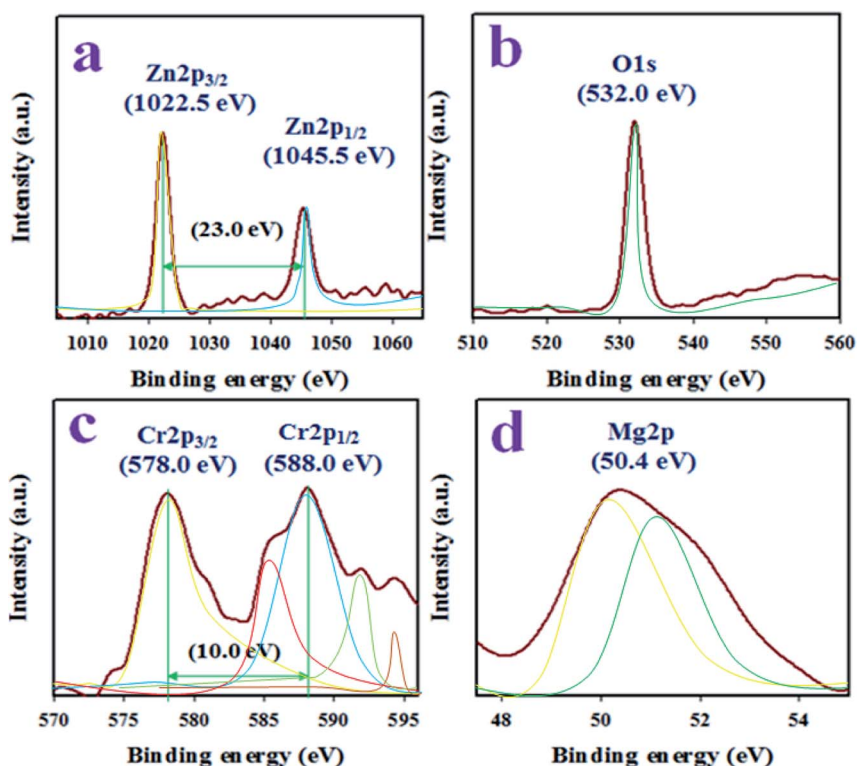


**Fig. 1** The XPS investigation to evaluate the ionization states and binding energy of the atoms in ZnO/MgO/Cr$_2$O$_3$ NFs. (a) The XPS spectra of the Zn 2p level orbital, (b) O 1s orbital, (c) core level Cr 2p orbital, and (d) Mg 2p orbital.
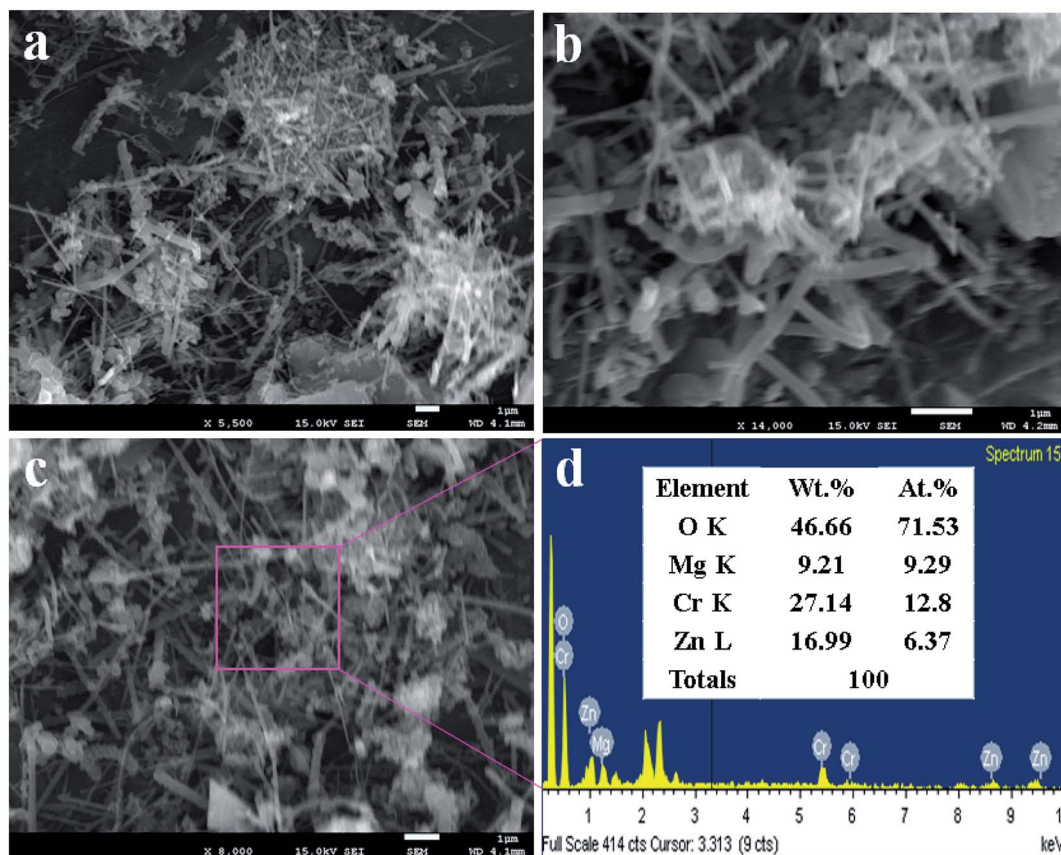
Fig. 2 The structural morphology and atomic compositions of the ZnO/MgO/Cr$_2$O$_3$ NFs obtained by FESEM analysis. (a and b) The low and high magnification FESEM images, (c) image of the EDS-confirmed nanofiber morphology of the ZnO/MgO/Cr$_2$O$_3$ nanocomposites, and (d) the elemental compositions of ZnO/MgO/Cr$_2$O$_3$ NFs analyzed by EDS.

for Cr$_2$O$_3$ are (104), (110), (122), and (306). These Cr$_2$O$_3$ phases were found to have very close similarity with JCPDS no. 038-1479 and reported articles.[50,51] Separately, the powder XRD patterns of ZnO and Cr$_2$O$_3$ were measured, and are presented in the same figure (Fig. 3(c)). The average grain sizes of the NFs were assessed at the NFs (104) peak using the Scherer equation, as shown in eqn (viii), and were found to be 42.51 nm:[52]

$$D = 0.9\lambda/(\beta \cos \theta) \qquad \text{(viii)}$$

where $\lambda$ is the wavelength of the X-ray radiation (1.5418 Å), and $\beta$ is the full width at half maximum (FWHM) of the peak at diffracted angle $\theta$.

## BET analysis

To investigate the surface area, pore volume, and pore diameter, BET analysis was performed on the synthesized NFs using the 3Flex analyzer (Micromeritics, USA) at 77.0 K. From the multi-point N$_2$ adsorption–desorption isotherm, the specific surface area of the ZnO/MgO/Cr$_2$O$_3$ NFs was calculated applying BET theory on the linear part of the BET-isotherm, as shown in Fig. 4. As shown in Fig. 4, the BET analysis report of the ZnO/MgO/Cr$_2$O$_3$ NFs shows the IV-type isotherm containing a hysteresis loop, which represented the mesoporous ordered

textural pores. Besides this, the BET report of the ZnO/MgO/Cr$_2$O$_3$ NFs exhibited a high surface area of 75.6 m$^2$ g$^{-1}$, 2.54 nm pore diameter and 0.034 cm$^3$ g$^{-1}$ pore volume. The surface area of the ZnO/MgO/Cr$_2$O$_3$ NFs indicated the case cavities that resulted in the reduction of the reactant chemical precursors using an alkaline medium.

## TEM analysis

In this approach, the morphology of the ZnO/MgO/Cr$_2$O$_3$ nanofibers was evaluated by TEM analysis. As observed from Fig. 5, the aggregated fiber-shaped morphology was exhibited in the ternary doped ZnO/MgO/Cr$_2$O$_3$ materials. The TEM images (Fig. 5(a–c)) show the ZnO/MgO/Cr$_2$O$_3$ nanofiber aggregated onto the surface of ternary materials, confirming the successful synthesis of the fiber materials of ZnO/MgO/Cr$_2$O$_3$. Therefore, it is very clear from the TEM images that the doped nanomaterial was assembled with fiber-like shaped morphology, which represents the aggregation as ternary nanostructure materials.

## Optimization and analyses of the ZnO/MgO/Cr$_2$O$_3$ NFs sensor performances

The working electrode of the desired toluene sensor probe was constructed with GCE coated by a thin uniform layer of wet-chemically prepared ZnO/MgO/Cr$_2$O$_3$ NFs. The required
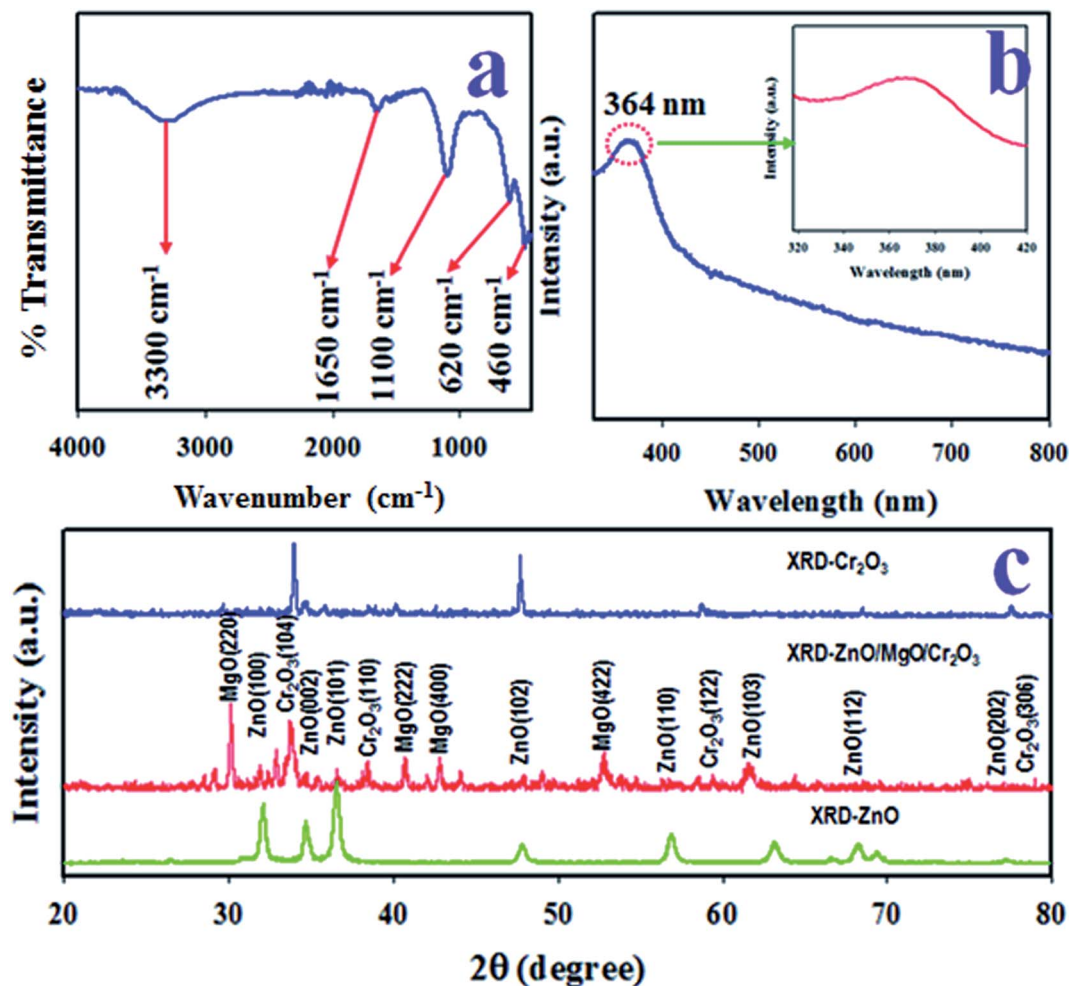
Fig. 3   Optical characterization of the ZnO/MgO/Cr$_2$O$_3$ NFs. (a) FTIR investigation to identify the existing functional groups in the synthesized NFs. (b) Evolution of the UV-Vis adsorption to calculate the optical band gap, and (c) the crystallinity and average grain size obtained from the XPD results.
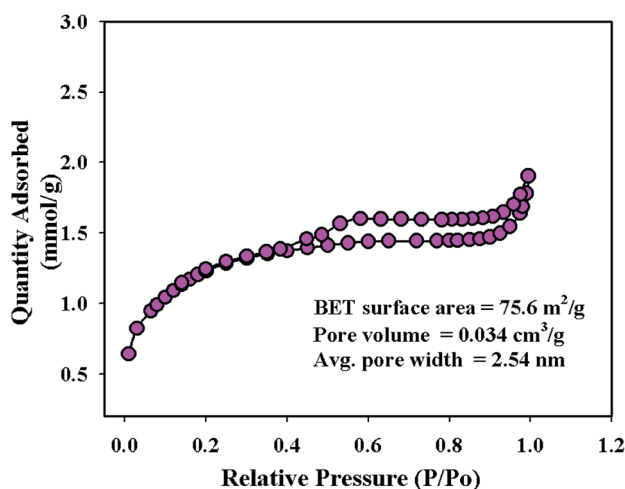


Fig. 4   Investigation of BET for ZnO/MgO/Cr$_2$O$_3$ nanofibers.

binding strength between the thin films of ZnO/MgO/Cr$_2$O$_3$ NFs and GCE was increased by the addition of Nafion adhesive. Due to the conductive nature of Nafion, it improves the conductance and electron transfer rate of the sensor reported previously.[52,53] In the electrochemical ($I$–$V$) analysis using the assembled sensor probe, the current density was measured on the surface of a thin film of ZnO/MgO/Cr$_2$O$_3$ NFs/GCE, and the holding time in the electrometer was set to 1 s as a constant throughout the experiment. To assess the selectivity of the sensor with the ZnO/MgO/Cr$_2$O$_3$ NFs/GCE electrode, the various environmental toxins with a concentration of 0.1 μM were analyzed at pH 7.0 in a potential range of 0 to +1.5 V. The resultant electrochemical responses of 2-acetylpyridin, M-xylol, 3-methylaniline, zimtaldehyde, 1,4-dioxane, toluene, chlorobenzene, hydroquinone, and paracetamol are presented in Fig. 6(a). Compared to the analyzed chemicals, toluene exhibited the uppermost electrochemical ($I$–$V$) response. According to the mechanism of the reaction (ix)–(xi), electrons are released in the aqueous system due to the oxidation of toluene on the surface of the ZnO/MgO/Cr$_2$O$_3$ NFs/GCE, which improved and enhanced the current
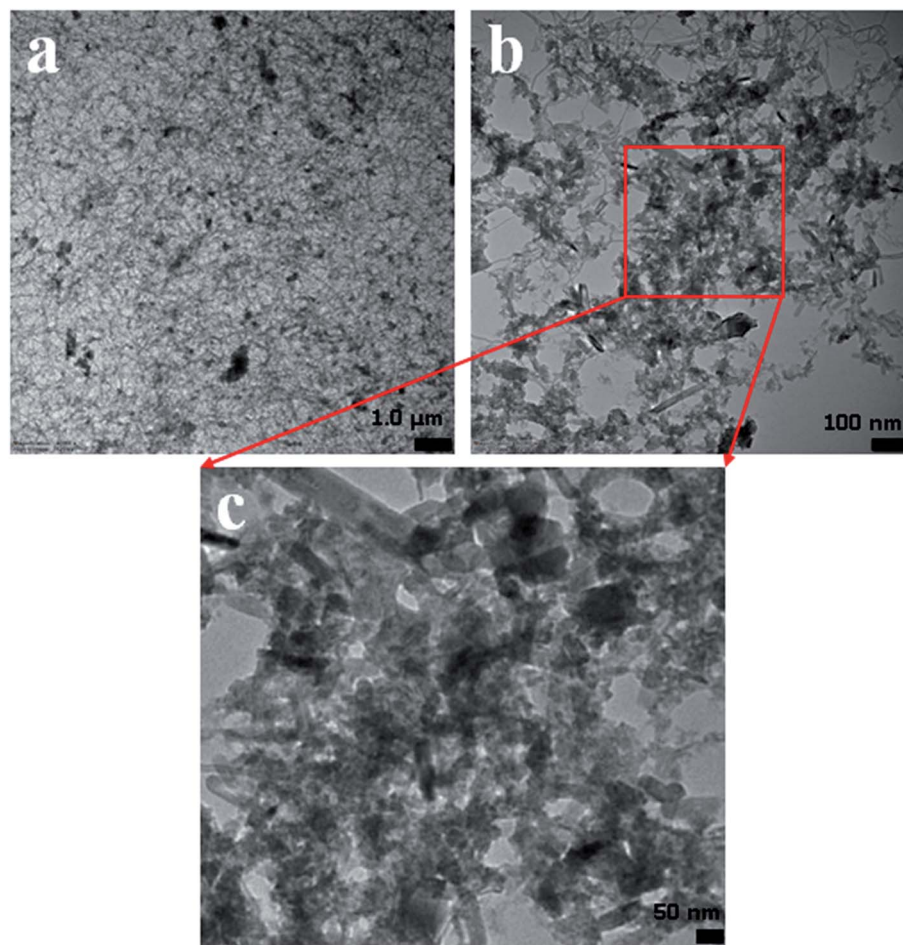
**Fig. 5** (a–c) TEM analysis from low to high magnification images of the ZnO/MgO/Cr$_2$O$_3$ nanofibers.

responses against the potential during the electrochemical measurement. As the highest I–V response is obtained from toluene, it is then considered as the selective analyte for the sensor probe.

It is not possible that the fabricated ZnO/MgO/Cr$_2$O$_3$ NFs/ GCE sensor probe would show the identical electrochemical result towards toluene analyte in the phosphate buffer solution in different pH. Therefore, the pH value optimization is necessary to obtain the maximum electrochemical outcome from the sensor. As a result, the fabricated sensor was subjected to analyze toluene in a wide pH range (5.7–8.0) of buffer solutions. The pH-dependent electrochemical responses of toluene with a concentration of 0.1 μM were studied at applied potentials of 0 to +1.5 V, as illustrated in Fig. 6(b). As shown in Fig. 6(b), the sensor based on the ZnO/MgO/Cr$_2$O$_3$ NFs/GCE was found to show the highest electrochemical response at pH 6.5 in the analysis of toluene. Thus, pH 6.5 is the optimum condition for the electrochemical oxidation of toluene on the assembled sensor probe.

After that, a series of toluene solutions with varying concentrations ranging from 0.1 mM to 0.1 nM were investigated at a potential of 0 to +1.5 V in the buffer solution of pH 6.5, and the resultant electrochemical responses are shown in

Fig. 6(c). As observed in Fig. 6(c), the electrochemical outcomes were amplified with increasing toluene concentration in the sensing buffer solution in a sequence of low to high, and distinguishable from each other. The similar tendency in the I– V responses have been observed in the detection of various toxins, as reported earlier.[54,55] To evaluate the analytical parameters, such as sensitivity, LDR, LOD, and LOQ of the projected toluene sensor, a linear relation of current *versus* toluene concentration was plotted, as shown in Fig. 6(d), and known as the calibration curve of the toluene sensor. For this plot, the current data were isolated at a potential of +1.5 V from Fig. 6(c). The sensor sensitivity was calculated from the slope of the calibration curve (0.7551 μA μM$^{-1}$) by considering the active surface area (0.0316 cm$^2$) of GCE. The estimated sensitivity was found to be 23.89 μA μM$^{-1}$ cm$^{-2}$. From the inset in Fig. 6(d), the current *versus* the logarithm of the concentration plot was found to be linear (regression co-efficient $R^2$ = 0.9958) in the range of 0.1 nM to 0.01 mM, which is defined as a linear dynamic range (LDR) of the sensor to toluene detection. Obviously, this LDR is wider. The LOD and LOQ of the toluene sensor based on ZnO/MgO/Cr$_2$O$_3$ NFs/GCE were computed using a signal/noise (S/N) ratio of 3, and the resultant values were equal to 95.59 ± 1.50 pM and 318.63 ± 2.0 pM,
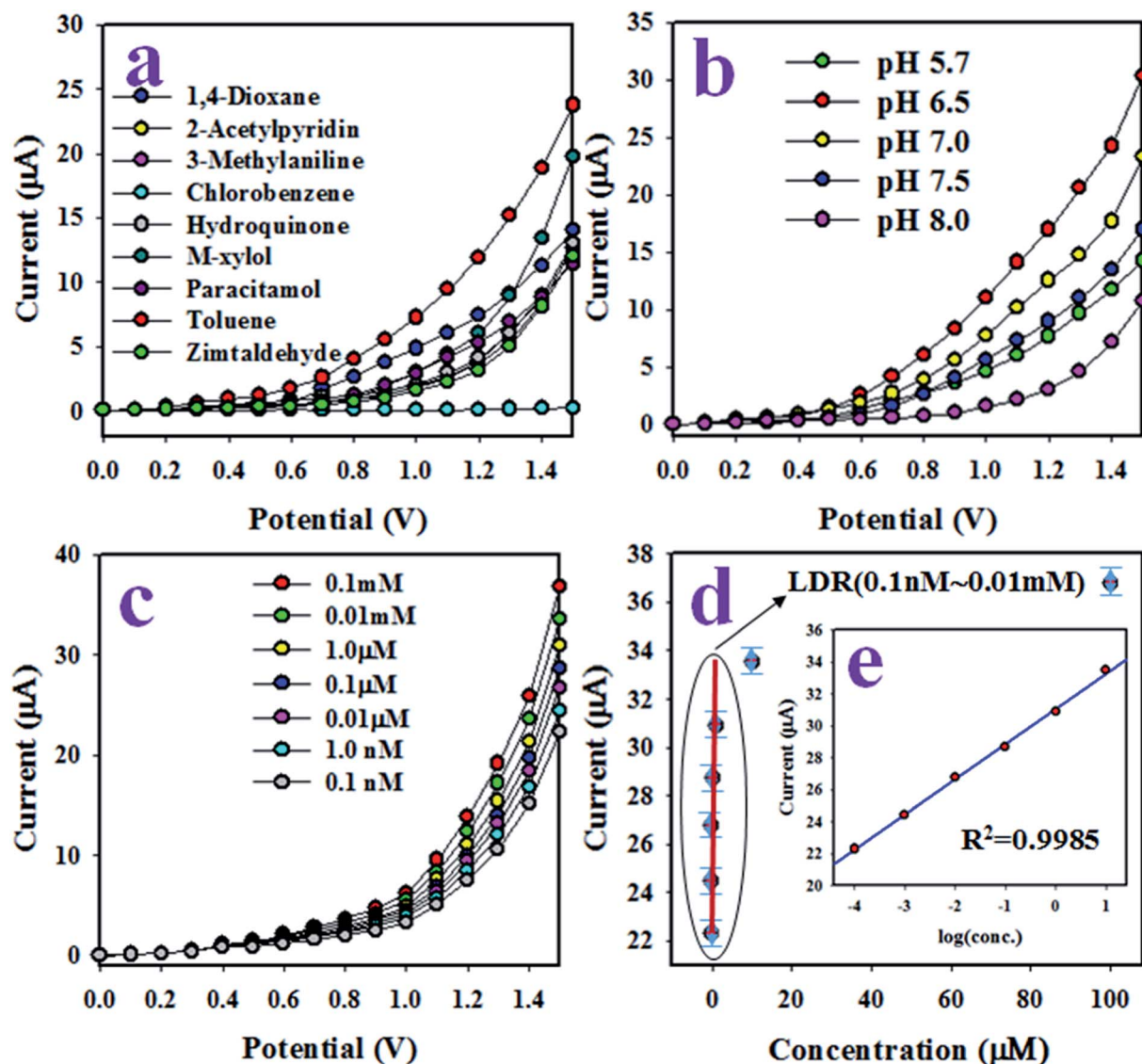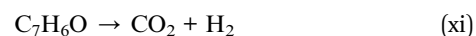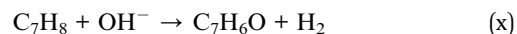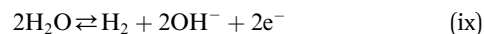
**Fig. 6** Optimization of the chemical sensor analytical performances of the ZnO/MgO/$Cr_2O_3$ NFs/GCE sensor probe, (a) selectivity assessment with analyte concentration of 0.1 μM, (b) pH optimization at 0.1 μM toluene, (c) electrochemical responses to toluene concentration, and (d) exploration of the calibration curve [inset: log(toluene-conc.) *vs.* current].

respectively. Thus, the resultant LOD and LOQ values are appreciably lower for toluene detection.

As observed in Fig. 6(d), the current responses were distributed evenly on a line. Therefore, it provided the evidence for the reliability of this method. Then, it was obvious that the ZnO/MgO/$Cr_2O_3$ NFs/GCE-based electrode could be used to determine the toluene level in buffer solutions in a wide range of concentrations. The proposed oxidation mechanism of toluene in the phosphate buffer system is illustrated in Scheme 1. In the *I–V* analysis, toluene is oxidized to generate free electrons, which are responsible for the enhancement of the conductance of the sensing buffer phase. As a result, the intensive electrochemical (*I–V*) response was detected. As shown in the reaction (ix)–(xi), the water molecules are adsorbed on the surface of the ZnO/MgO/$Cr_2O_3$ NFs/GCE electrode, and $OH^-$, $H_2$ and electrons are generated. Subsequently, $OH^-$ is reacted with $C_7H_8$ to

produce $C_6H_6O$ and finally, $CO_2$ and $H_2$. The similar electrochemical oxidation of toluene has been reported earlier.[56,57]

$$2H_2O \rightleftharpoons H_2 + 2OH^- + 2e^- \qquad \text{(ix)}$$

$$C_7H_8 + OH^- \rightarrow C_7H_6O + H_2 \qquad \text{(x)}$$

$$C_7H_6O \rightarrow CO_2 + H_2 \qquad \text{(xi)}$$

The response time is a tool to evaluate the efficiency of an electrochemical sensor, and is defined as the time required to complete an electrochemical analysis of an analyte. Therefore, the response time of the toluene sensor with ZnO/MgO/$Cr_2O_3$ NFs/GCE was tested with 0.1 μM toluene at a potential of 0 to +1.5 V in the buffer solution, and the result is shown in Fig. 7(a).
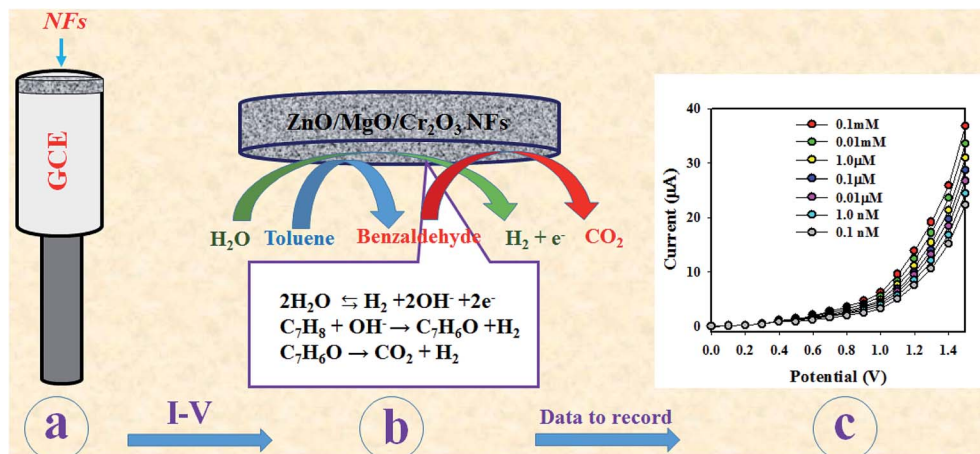
**Scheme 1** Schematic representation of the sensing mechanism to detect toluene by ZnO/MgO/Cr$_2$O$_3$ NFs/GCE during electrochemical analysis. (a) The modification process of GCE with NFs, (b) the $I$–$V$ detection of toluene, and (c) the resultant data to record at the electrometer.

As in Fig. 6(a), the response time was achieved at 18.0 s, which is appreciable and provides the information about the high efficiency of the toluene sensor probe. Fig. 7(b) shows the electrochemical responses of the various modified GCE with ZnO/MgO/Cr$_2$O$_3$ NFs, ZnO/MgO NPs, ZnO/Cr$_2$O$_3$ NPs, ZnO NPs, MgO NPs and Cr$_2$O$_3$ NPs in identical conditions (0.01 μM toluene analyte concentration; applied potential range of 0 to +1.5 V; phosphate butter phase at pH 6.5. The GCE is modified by a ternary mixture of ZnO/MgO/Cr$_2$O$_3$ NFs, and shows the superlative $I$–$V$ response compared to the binary ZnO/MgO NPs, ZnO/Cr$_2$O$_3$ NPs, and single ZnO NPs, MgO NPs and Cr$_2$O$_3$ NPs. It occurred owing to the combinational effects of the co-doped ternary metal oxides. The other cause is that the conductivity of the mixed metal oxides is increased compared to the single or binary NPs. As a result, the ZnO/MgO/Cr$_2$O$_3$ NFs showed the highest electrochemical activity toward toluene (analyte), as shown in Fig. 7(b). The reproducibility performance of the toluene sensor was tested in 0.01 μM toluene in the buffer at pH 6.5 (potential range: 0 to +1.5 V). As observed in Fig. 7(c), the replicated seven runs are practically undistinguishable in identical conditions, which confirmed the evidence of the consistency of the toluene chemical sensor with the ZnO/MgO/Cr$_2$O$_3$ NFs fabricated sensor probe. The magnitude of the electrochemical responses of the reproducibility test was not altered even after washing the electrode with PBS buffer in each run. The precision of the current data of the reproducibility test at a potential of +1.5 V was calculated, and found to be ±0.59% in the form of a relative standard deviation (RSD). It provided evidence of the high precision of reproducibility of the selective toluene electrochemical sensor. The tests under the identical conditions of concentration of target toluene, pH of the medium, and applied potential were executed for reproducibility. They were performed for an extended period in consecutive seven days, and are presented in Fig. 6(d). The relative standard deviation (RSD) of the current data of these tests at +1.5 V was calculated, and it was found as ±1.0%. In conclusion, the toluene sensor with ZnO/MgO/Cr$_2$O$_3$ NFs/GCE showed long-term stability with high precision in sensing performance.

It is shown in Fig. 5(c) that the current density measured in the buffer system is directly proportional to the corresponding concentration of toluene.

Thus, the amplified $I$–$V$ responses were observed with increasing toluene concentration. At the very beginning of the toluene detection performance, the surface coverage with the adsorption of a few numbers of analyte (toluene) molecules was smaller. In addition, the oxidation reaction of toluene on the surface of the working electrode was started progressively. With the enhancement of toluene molecules, the surface reaction and coverage both increased gradually and approached its equilibrium saturation state. Furthermore, the enhancement of the toluene concentration in the sensing buffer medium, a steady-state current density and the reaction rate were attained. Such steady-state equilibrium data are shown in Fig. 6(d), where the current data are scattered on a line. Therefore, the projected toluene sensor with ZnO/MgO/Cr$_2$O$_3$ NFs/GCE was able to detect and quantify the targeted analyte (toluene) in the real-field of its application. Previously, it has been projected that the response time of the toluene chemical sensor is around 18.0 s, and some reserve time of 20.0 s is needed to attain the steady-state equilibrium $I$–$V$ response, as shown in Fig. 7(a). As demonstrated in Fig. S1 and S2 in the ESI section (ESM), Fig. S1(a)† presents the three individual $I$–$V$ responses of toluene, M-xylol and 1,4-dioxane, respectively, which are completely distinguishable. On the other hand, Fig. S1(b)† illustrates the four $I$–$V$ responses, such as 'toluene', 'toluene & M-xylol', 'toluene & 1,4-dioxane' and 'toluene, M-xylol & 1,4-dioxane', which are indistinguishable. Therefore, these tests provided evidence that the ZnO/MgO/Cr$_2$O$_3$ NFs/GCE chemical sensor is selective to toluene, and there is no measurable interference effect in the presence of another toxin in the measuring system. Therefore, the toluene chemical sensor with ZnO/MgO/Cr$_2$O$_3$ NFs/GCE is a promising sensor to detect toluene selectively, reliably and precisely in the real environment of its application. Nafion has no significant role in the sensing of the target analyte with the ZnO/MgO/Cr$_2$O$_3$ NFs/GCE sensor probe in the $I$–$V$ measurement. In addition,
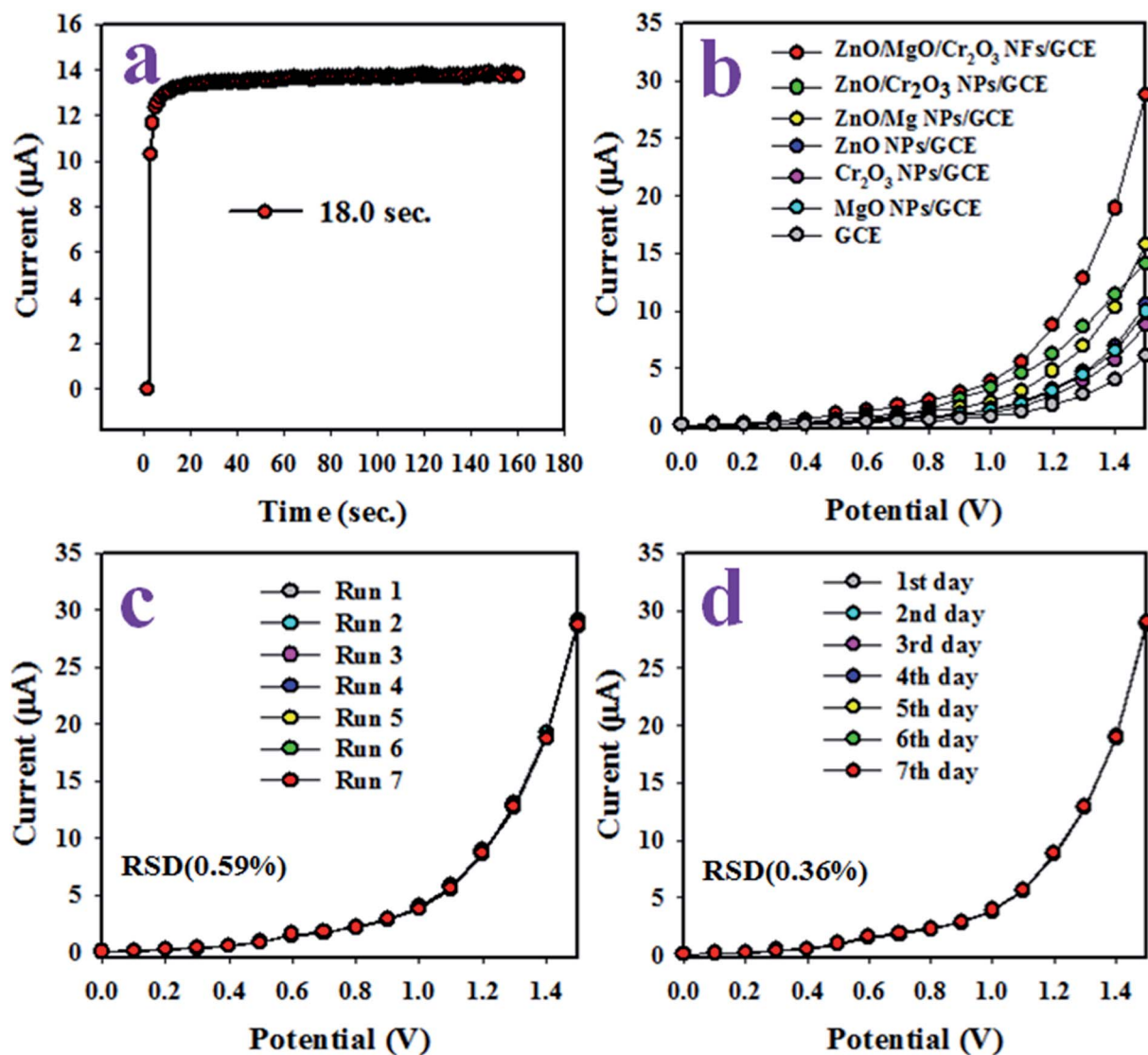
Fig. 7 Assessment of the reliability parameters of the toluene sensor with ZnO/MgO/Cr$_2$O$_3$ NFs/GCE. (a) The assessment of the response time of the toluene sensor at 0.1 μM. (b) The comparison between the electrochemical responses of the sensor with GCE modified by single, binary and ternary metal oxides at 0.01 μM toluene and pH 6.5. (c) The reproducibility parameter tested at 0.1 μM, and (d) the long-time performance ability test of the toluene sensor.

a control experiment was executed with the various modification electrodes (Bare GCE, Nafion/GCE, and ZnO/MgO/Cr$_2$O$_3$ NFs/GCE), which is included in the ESM (Fig. S2†). There are no significant changes in the electrochemical signal without and with the Nafion binder during the detection of the target analyte. Here, Nafion is used as a chemical glue to stick the nanofibers onto the GCE. The reliability and stability of the fabricated ZnO/MgO/Cr$_2$O$_3$ NFs were studied, and are included in the ESI section (Fig. S3†). The I–V experiment was carried out with the same ZnO/MgO/Cr$_2$O$_3$ NFs-modified GCE electrode

Table 1 The comparison of the analytical performances of the proposed toluene sensor with similar works

| Electrode | Analyte | DL[a] | LDR[b] | Sensitivity | Ref. |
|---|---|---|---|---|---|
| ZnO/Yb$_2$O$_3$NSs/GCE | 4-Aminophenol | 94 pM | 1.0 nM–0.1 mM | 5.06 μA μM$^{-1}$ cm$^{-2}$ | 9 |
| MnCo$_x$O$_y$ NPs/GCE | 3,4-Diaminotoluene | 0.26 pM | 1.0 pM–1.0 μM | 0.37 μA μM$^{-1}$ cm$^{-2}$ | 59 |
| FeO/CdO NCs/GCE | 1,2-Dichlorobenzene | 72.73 nM | 0.089 nM–8.9 mM | 1.31 μA μM$^{-1}$ cm$^{-2}$ | 60 |
| ZnO/MgO/Cr$_2$O$_3$ NFs/GCE | Toluene | 95.59 pM | 0.1 nM–0.01 mM | 23.89 μA μM$^{-1}$ cm$^{-2}$ | This report |

[a] DL (detection limit). [b] LDR (linear dynamic range), pM (picomolar), mM (millimolar).

**Table 2** The electrochemical analysis of real samples with ZnO/MgO/Cr$_2$O$_3$ NFs/GCE probe applying the electrochemical approach

| Real samples | Added tol conc. (µM) | Measured toluene conc. by ZnO/MgO/Cr$_2$O$_3$ NFs/GCE$^a$ (µM) | | | Average recovery$^b$ (%) | RSD$^c$ ($n = 3$) (%) |
|---|---|---|---|---|---|---|
| | | $R_1$ | $R_2$ | $R_3$ | | |
| Industrial effluent | 0.01000 | 0.009494 | 0.009405 | 0.009573 | 94.91 | 0.89 |
| PC-baby bottle | 0.01000 | 0.009832 | 0.01001 | 0.009827 | 98.89 | 1.05 |
| PVC-water bottle | 0.01000 | 0.009783 | 0.009589 | 0.009613 | 96.62 | 1.09 |
| PVC-food packaging bag | 0.01000 | 0.009593 | 0.009571 | 0.009680 | 96.15 | 0.60 |
| Sea water | 0.01000 | 0.009350 | 0.009047 | 0.009192 | 91.96 | 1.65 |

$^a$ Mean of three repeated determination (signal to noise ratio 3) with ZnO/MgO/Cr$_2$O$_3$ NFs/GCE. $^b$ Concentration of toluene determined/concentration taken (unit: µM). $^c$ Relative standard deviation value indicates precision among three repeated measurements ($R_1$, $R_2$, $R_3$).

under identical conditions in seven consecutive days. The electrochemical responses were observed with similar results for the detection of the target toluene analyte, and are presented in Fig. S3a.† So, after seven days, the electrochemical response was found to be almost the same as the previous results. On the other hand, the stability of the ZnO/MgO/Cr$_2$O$_3$ NFs-fabricated GCE was also evaluated in the ferrocyanide couples using voltammograms under identical conditions. It was observed that the fabricated ZnO/MgO/Cr$_2$O$_3$ NFs/GCE sensor probe showed almost the same response after 20 cycles, which is presented in Fig. S3b.† Therefore, it is concluded that the fabricated ZnO/MgO/Cr$_2$O$_3$ NFs/GCE sensor probe is very reliable, as well as stable, even after several cycles and days. The ZnO/MgO/Cr$_2$O$_3$ NFs as an electron mediator can provide a satisfactory nanoenvironment due to its high crystalline phases with the average molecular size of 42.51 nm, which can offer the successful detection of toluene in the phosphate buffer phase. The synthesized nanofiber of ZnO/MgO/Cr$_2$O$_3$ also exhibited the average band-gap energy of 3.41 eV, which facilitated the high electron transfer from the active sites of the NFs toward the GCE. As a result, the assembled sensor established a good electron communication to detect toluene in the buffer solution in the electrochemical ($I$–$V$) approach. In Table 1,[9,58,59] the sensing parameters of the formerly studied electrochemical sensor based on different nanomaterial matrices are illustrated. Among these, the tested toluene sensor based on ZnO/MgO/Cr$_2$O$_3$ NFs/GCE showed appreciable performances.

### Analyses of real environmental samples

The standard recovery test of the proposed toluene chemical sensor probe based on ZnO/MgO/Cr$_2$O$_3$ NFs/GCE was performed by using an electrochemical ($I$–$V$) approach. To investigate the analysis, a known concentration of the target toluene solution was added to the collected real samples. The resultant data were systematically investigated to measure the concentration of the target toluene again, which was calculated as % recovery. In this analysis, the environmental samples were collected and extracted from different sources, such as seawater, PC-baby bottle, PVC-food packaging bag, PVC-water bottle, and waste effluent from the industrial area. The resulting data are summarized in Table 2. The results for the validation of the fabricated sensor were found to be quite acceptable.

## Conclusion

The selective toluene electrochemical sensor was prepared by GCE coated with calcined ZnO/MgO/Cr$_2$O$_3$ NFs as the layer of thin-film using 5% Nafion adhesive. The proposed sensor was found to be reliable in determining the toluene level in PBS (buffer solution) medium. It shows the excellent responses in terms of the sensitivity, DOL, LOQ, LDR, reproducibility, and stability. Besides this, it is a successful sensor in the detection of toluene in real wastewater polluted samples by the recovery method. Therefore, this research work might be a noble approach for the development of a future chemical sensor probe to identify unsafe toxins in the environmental safety and health care sectors in broad scales.

## Conflicts of interest

There are no conflicts to declare.

## Acknowledgements

## References

1 T. Ueda, H. Abe, K. Kamad, S. R. Bishop, H. L. Tuller, T. Hyodo and Y. Shimizu, Enhanced sensing response of solid–electrolyte gas sensors to toluene: Role of composite Au/metal oxide sensing electrode, *Sens. Actuators, B*, 2017, **252**, 268–276.
2 C. Dong, X. Liu, X. Xiao, S. Du and Y. Wang, Monodisperse ZnFe$_2$O$_4$ nanospheres synthesized by a nonaqueous route for a highly selective low-ppm-level toluene gas sensor, *Sens. Actuators, B*, 2017, **239**, 1231–1236.
3 V. S. Vaishnav, S. G. Patel and J. N. Panchal, Development of indium tin oxide thin film toluene sensor, *Sens. Actuators, B*, 2015, **210**, 165–172.
4 D. James, S. M. Scott, Z. Ali and W. T. O'Hare, Chemical Sensors for Electronic Nose Systems, *Microchim. Acta*, 2005, **149**, 1–17.

5   R. Rajamanickam, K. Kaliyamoorthi, N. Ramachandran, D. Baskaran and J. Krishnan, Batch biodegradation of toluene by mixed microbial consortia and its kinetics, *Int. Biodeterior. Biodegrad.*, 2017, **119**, 282–288.

6   D. I. Lubman and M. Yücel, Drugs, mental health and the adolescent brain: plications for early intervention, *Early Intervention in Psychiatry*, 2008, **2**, 63–66.

7   B. E. Perron and M. O. Howard, Adolescent inhalant use, abuse and dependence, *Addiction*, 2009, **104**, 1185–1192.

8   M. M. Rahman, M. M. Alam, A. M. Asiri and M. A. Islam, Ethanol sensor development based on ternary-doped metal oxides (CdO/ZnO/Yb$_2$O$_3$) nanosheets for environmental safety, *RSC Adv.*, 2017, **7**, 22627–22639.

9   M. M. Rahman, M. M. Alam, A. M. Asiri and M. R. Awual, Fabrication of 4-aminophenol sensor based on hydrothermally prepared ZnO/Yb$_2$O$_3$ nanosheets, *New J. Chem.*, 2017, **41**, 9159–9169.

10  M. M. Rahman, M. M. Alam and A. M. Asiri, Fabrication of an acetone sensor based on facile ternary MnO$_2$/Gd$_2$O$_3$/SnO$_2$ nanosheets for environmental safety, *New J. Chem.*, 2017, **41**, 9938–9946.

11  H. Ma, Y. Xu, Z. Rong, X. Cheng, S. Gao and X. Zhang, Highly toluene sensing performance based on monodispersed Cr$_2$O$_3$ porous microspheres, *Sens. Actuators, B*, 2012, **174**, 325–331.

12  L. W. Wang, S. R. Wang, M. J. Xu, X. J. Hu, H. X. Zhang, Y. S. Wang and W. P. Huang, A Au-functionalized ZnO nanowire gas sensor for detection of benzene and toluene, *Phys. Chem. Chem. Phys.*, 2013, **15**, 17179–17186.

13  J. R. Huang, X. J. Xu, C. P. Gu, W. Z. Wang, B. Y. Geng, Y. F. Sun and J. H. Liu, Effective VOCs gas sensor based on porous SnO2 microcubes prepared *via* spontaneous phase segregation, *Sens. Actuators, B*, 2012, **173**, 599–606.

14  Z. H. Li, J. C. Li, L. L. Song, H. Q. Gong and Q. Niu, Ionic liquid-assisted synthesis of WO3 particles with enhanced gas sensing properties, *J. Mater. Chem. A*, 2013, **1**, 15377–15382.

15  S. R. Wang, Y. S. Wang, H. X. Zhang, X. L. Gao, J. D. Yang and Y. Wang, Fabrication of porous α-Fe$_2$O$_3$ nanoshuttles and their application for toluene sensors, *RSC Adv.*, 2014, **4**, 30840–30849.

16  C. H. Zhao, B. Y. Huang, J. Y. Zhou and E. Q. Xie, Synthesis of porous Co3O4 nanonetworks to detect toluene at low concentration, *Phys. Chem. Chem. Phys.*, 2014, **16**, 19327–19332.

17  Z. Li, Y. Li, Y. Luan, J. Li and A. Song, (OH)$_3$ particles from an ionic liquid precursor and their conversion to porous In2O3 particles for enhanced gas sensing properties, *CrystEngComm*, 2013, **15**, 1706–1714.

18  J. H. Kim and S. S. Kim, Dual Functional Sensing Mechanism in SnO2–ZnO Core–Shell Nanowires, *ACS Appl. Mater. Interfaces*, 2015, **7**, 17199–17208.

19  H. Shan, C. B. Liu, L. Liu, J. B. Zhang, H. Y. Li, Z. Liu, X. B. Zhang and X. Q. Chi, Excellent Toluene Sensing Properties of SnO2–Fe2O3 Interconnected Nanotubes, *ACS Appl. Mater. Interfaces*, 2013, **5**, 6376–6380.

20  D. X. Ju, H. Y. Xu, Z. W. Qiu, Z. C. Zhang, Q. Xu, J. Zhang, J. Q. Wang and B. Q. Cao, Near Room Temperature, Fast-Response, and Highly Sensitive Triethylamine Sensor Assembled with Au-Loaded ZnO/SnO2 Core–Shell Nanorods on Flat Alumina Substrates, *ACS Appl. Mater. Interfaces*, 2015, **7**, 19163–19171.

21  Y. Cui, A. Yu, H. Pan, X. Zhou and W. Ding, Catalytic outgrowth of SnO2nanorods from ZnO–SnO2 nanoparticles microsphere core: combustion synthesis and gas-sensing properties, *CrystEngComm*, 2012, **14**, 7355–7359.

22  H. Woo, C. W. Na, I. D. Kim and J. Lee, Highly sensitive and selective trimethylamine sensor using one-dimensional ZnO–Cr$_2$O$_3$ hetero-nanostructures, *Nanotechnology*, 2012, **23**, 24.

23  C. Lee, I. D. Kim and J. Lee, Selective and sensitive detection of trimethylamine using ZnO–In2O3 composite nanofibers, *Sens. Actuators, B*, 2013, **181**, 463–470.

24  H. E. Brown, The exciton spectrum of zinc oxide, *J. Phys. Chem. Solids*, 1960, **15**, 86–96.

25  O. Lupan, T. Pauporte, L. Chow, B. Viana, F. Pelle, L. K. Ono, B. R. Cuenya and H. Heinrich, Effects of annealing on properties of ZnO thin films prepared by electrochemical deposition in chloride medium, *Appl. Surf. Sci.*, 2010, **256**, 1895–1907.

26  G. R. A. Kumara, M. Okuya, K. Murakami, S. Kaneko, V. V. Jayaweera and K. J. Tennakone, Dye-sensitized solid-state solar cells made from magnesium oxide-coated nanocrystalline titanium dioxide films: enhancement of the efficiency, *J. Photochem. Photobiol., A*, 2004, **164**, 183–185.

27  S. W. Choi, A. Katoch, J. H. Kim and S. S. Kim, Prominent Reducing Gas-Sensing Performances of n-SnO2 Nanowires by Local Creation of p–n Heterojunctions by Functionalization with p-Cr2O3 Nanoparticles, *ACS Appl. Mater. Interfaces*, 2014, **6**, 17723–17729.

28  M. R. Awual, A. Islam, M. M. Hasan, M. M. Rahman, A. M. Asiri, M. A. Khaleque and M. C. Sheikh, Introducing an alternate conjugated material for enhanced lead (II) capturing from wastewater, *J. Cleaner Prod.*, 2019, **224**, 920–929.

29  M. R. Awual, M. M. Hasan, A. Islam, A. M. Asiri and M. M. Rahman, Optimization of an innovative composited material for effective monitoring and removal of cobalt (II) from wastewater, *J. Mol. Liq.*, 2020, **298**, 112035.

30  M. R. Awual, M. M. Hasan, M. M. Rahman and A. M. Asiri, Novel composite material for selective copper (II) detection and removal from aqueous media, *J. Mol. Liq.*, 2019, **283**, 772–780.

31  J. G. Speight, *Lange's Handbook of Chemistry 1*, McGraw-Hill, New York, 16th edn, 2005, pp. 1.331–1.342.

32  J. Zhang, D. Gao, G. Yang, J. Zhang, Z. Shi, Z. Zhang, Z. Zhu and D. Xue, Synthesis and magnetic properties of Zr doped ZnO Nanoparticles, *Nanoscale Res. Lett.*, 2011, **6**, 587.

33  R. Yousefi, Effects of Sn atoms on formation of ZnO nanorings, *CrystEngComm*, 2015, **17**, 2698–2704.

34  D. Xu, D. Fan and W. Shen, Catalyst-free direct vapor-phase growth of Zn$_{1-x}$Cu$_x$O micro-cross structures and their optical properties, *Nanoscale Res. Lett.*, 2013, **8**, 46.

35  F. Wang, X. Cai, D. Yan, Z. Zhu, S. Xiao and X. Gu, Synthesis and cathodoluminescence characteristics of caltrop-like

ZnO nanostructures, *Superlattices Microstruct.*, 2014, **72**, 83–90.

36 L. Lu, C. Xiang, Y. He, F. Wang and S. Hu, Early hydration of C$_3$S in the presence of Cd$^{2+}$, Pb$^{2+}$ and Cr$^{3+}$ and the immobilization of heavy metals in pastes, *Constr. Build. Mater.*, 2017, **152**, 923–932.

37 J. Xu, Q. Yang, M. S. Javed, Y. Gong, M. K. Aslam and C. Chen, The effects of NaF concentration on electrochemical and corrosion behavior of AZ31B magnesium alloy in a composite electrolyte, *RSC Adv.*, 2017, **7**, 5880–5887.

38 H. C. Lee, Y. C. Huang, T. F. Liu, W. T. Whang and C. G. Chao, Effect of phosphate surface pretreatment on corrosion resistance and adhesion of PI coating on Mg-5 wt% Sn alloy, *J. Adhes. Sci. Technol.*, 2015, **29**, 1229–1245.

39 R. Augustine, E. A. Dominic, I. Reju, B. Kaimal, N. Kalarikkal and S. Thomas, Investigation of angiogenesis and its mechanism using zinc oxide nanoparticle-loaded electrospun tissue engineering scaffolds, *RSC Adv.*, 2014, **4**, 51528–51536.

40 K. Thangavel, A. Balamurugan, T. Venkatachalam and E. R. Kumar, Structural, morphological and optical properties of ZnO nano-fibers, *Superlattices Microstruct.*, 2016, **90**, 45–52.

41 S. Hayashi, N. Nakamori and H. Kanamori, Generalized Theory of Average Dielectric Constant and Its Application to Infrared Absorption by ZnO Small Particles, *J. Phys. Soc. Jpn.*, 1979, **46**, 176–183.

42 P. Li, C. Liu, I. Zhang, S. Zheng and Y. Zhang, Enhanced boron adsorption onto synthesized MgO nanosheets by ultrasonic method, *Ultrason. Sonochem.*, 2017, **34**, 938–946.

43 L. Peia, W. Y. Yin, J. F. Wang, J. Chen, C. G. Fan and Q. F. Zhang, Low temperature synthesis of magnesium oxide and spinel powders by a sol–gel process, *Mater. Res.*, 2010, **13**, 339–343.

44 R. M. R. Junqueira, C. R. O. Loureiro, M. S. Andrade and V. T. L. Buono, Characterization of interference thin films grown on stainless steel surface by alternate pulse current in a sulphochromic solution, *Mater. Res.*, 2008, **11**, 421–426.

45 D. K. Bhat, Facile Synthesis of ZnO Nanorods by Microwave Irradiation of Zinc–Hydrazine Hydrate Complex, *Nanoscale Res. Lett.*, 2008, **3**, 31.

46 M. R. Arefi and S. R. Zarchi, Synthesis of zinc oxide nanoparticles and their effect on the compressive strength and setting time of self-compacted concrete paste as cementitious composites, *Int. J. Mol. Sci.*, 2012, **13**, 4340–4350.

47 C. Ma, Z. Zhou, H. Wei, Z. Yang, Z. Wang and Y. Zhang, Rapid large-scale preparation of ZnO nanowires for photocatalytic application, *Nanoscale Res. Lett.*, 2011, **6**, 536.

48 A. Fakhri and S. Behrouz, Comparison studies of adsorption properties of MgO nanoparticles and ZnO–MgO nanocomposites for linezolid antibiotic removal from aqueous solution using response surface methodology, *Process Saf. Environ. Prot.*, 2015, **94**, 37–43.

49 I. Elahi, R. Zahir, K. Mehmood, A. Jamil and N. Amin, Co-precipitation synthesis, physical and magnetic properties of manganese ferrite powder, *Afr. J. Pure Appl. Chem.*, 2012, **6**, 1–5.

50 P. Gibot, F. Schnell and D. Spitzer, Ca$_3$(PO$_4$)$_2$ biomaterial: A nontoxic template to prepare highly porous Cr$_2$O$_3$, *Mater. Lett.*, 2015, **161**, 172–174.

51 D. N. Suryawanshi, D. R. Patil and L. A. Patil, Fe$_2$O$_3$-activated Cr$_2$O$_3$ thick films as temperature dependent gas sensors, *Sens. Actuators, B*, 2008, **134**, 579–584.

52 M. M. Alam, A. M. Asiri, M. T. Uddin, M. A. Islam and M. M. Rahman, Wet-chemically prepared low-dimensional ZnO/Al$_2$O$_3$/Cr$_2$O$_3$ nanoparticles for xanthine sensor development using an electrochemical method, *RSC Adv.*, 2018, **8**, 12562–12572.

53 M. M. Alam, A. M. Asiri, M. T. Uddin, M. A. Islam, M. R. Awual and M. M. Rahman, Detection of uric acid based on doped ZnO/Ag$_2$O/Co$_3$O$_4$ nanoparticle loaded glassy carbon electrode, *New J. Chem.*, 2019, **43**, 8651–8659.

54 M. M. Alam, A. M. Asiri, M. T. Uddin, Inamuddin, M. A. Islam, M. R. Awual and M. M. Rahman, One-step wet-chemical synthesis of ternary ZnO/CuO/Co$_3$O$_4$ nanoparticles for sensitive and selective melamine sensor development, *New J. Chem.*, 2019, **43**, 4849–4858.

55 B. M. Abu-Zied, M. M. Alam, A. M. Asiri, W. Schwieger and M. M. Rahman, Fabrication of 1,2-dichlorobenzene sensor based on mesoporous MCM-41 material, *Colloids Surf., A*, 2019, **562**, 161–169.

56 Q. Shang, X. Tan, T. Yu, Z. Zhang, Y. Zou and S. Wang, Efficient gaseous toluene photoconversion on graphene–titanium dioxide nanocomposites with dominate exposed {0 0 1} facets, *J. Colloid Interface Sci.*, 2015, **455**, 134–144.

57 M. M. Alam, A. M. Asiri, M. T. Uddin, M. A. Isalm, M. R. Awual and M. M. Rahman, In-situ Glycine Sensor Development Based ZnO/Al$_2$O$_3$/Cr$_2$O$_3$ Nanoparticles, *ChemistrySelect*, 2018, **3**, 11460–11468.

58 A. Lannoy, N. Kania, R. Bleta, S. Fourmentin, C. M. Binkowski, E. Monflier and A. Ponchel, Photocatalysis of Volatile Organic Compounds in water: Towards a deeper understanding of the role of cyclodextrins in the photodegradation of toluene over titanium dioxide, *J. Colloid Interface Sci.*, 2016, **461**, 317–325.

59 M. M. Rahman, M. M. Alam, A. M. Asiri and M. A. Islam, 3,4-Diaminotoluene sensor development based on hydrothermally prepared MnCoxOy nanoparticles, *Talanta*, 2018, **176**, 17–25.

60 M. M. Rahman, M. M. Alam and A. M. Asiri, Sensitive 1,2-dichlorobenzene chemi-sensor development based on solvothermally prepared FeO/CdO nanocubes for environmental safety, *J. Ind. Eng. Chem.*, 2018, **62**, 392–400.